1   **MAVS mediates a protective immune response in the brain to Rift Valley fever virus**
2
3   Nicholas R. Hum[1], Feliza A. Bourguet[1], Aimy Sebastian[1], Doris Lam[1], Ashlee M. Phillips[1],
4   Kristina R. Sanchez[1, #a], Amy Rasley[1], Gabriela G. Loots[1,2], Dina R. Weilhammer[1*]
5
6
7   [1] Biosciences and Biotechnology Division, Lawrence Livermore National Laboratory,
8   Livermore, CA, USA
9   [2] School of Natural Sciences, University of California Merced, Merced, CA 94550, USA
10   [#a]Current address: Immunology Graduate Group, University of California, Davis, Davis, CA
11   95616, USA
12
13
14   *Corresponding author
15   Email: weilhammer1@llnl.gov
16
17   Short title: Innate immunity in the brain to Rift Valley fever virus
18
19   Keywords:
20   Rift Valley fever virus, microglia, MAVS, scRNA-seq, IFN signaling,
21
22

Abstract

Rift Valley fever virus (RVFV) is a highly pathogenic mosquito-borne virus capable of causing hepatitis, encephalitis, blindness, hemorrhagic syndrome, and death in humans and livestock. Upon aerosol infection with RVFV, the brain is a major site of viral replication and tissue damage, yet pathogenesis in this organ has been understudied. Here, we investigated the immune response in the brain of RVFV infected mice. In response to infection, microglia initiate robust transcriptional upregulation of antiviral immune genes, as well as increased levels of activation markers and cytokine secretion that is dependent on mitochondrial antiviral-signaling protein (MAVS) and independent of toll-like receptors 3 and 7. *In vivo*, *Mavs*$^{-/-}$ mice displayed enhanced susceptibility to RVFV as determined by increased brain viral burden and higher mortality. Single-cell RNA sequence analysis identified microglia-specific defects in type I interferon and interferon responsive gene expression in *Mavs*$^{-/-}$ mice, as well as dysregulated lymphocyte infiltration. The results of this study provide a crucial step towards understanding the precise molecular mechanisms by which RVFV infection is controlled in the brain and will help inform the development of vaccines and antiviral therapies that are effective in preventing encephalitis.

Author Summary

Rift Valley fever virus causes severe disease in humans and livestock and in some cases can be fatal. There is concern about the use of Rift Valley fever virus as a bioweapon since it can be transmitted through the air, and there are no vaccines or antiviral treatments. Airborne transmission of the virus causes severe inflammation of the brain, yet little is known about the immune response against the virus in this organ. Here, we investigated the immune response in the brain to Rift Valley fever virus following intranasal infection. We determined that microglia, the resident immune cells of the brain, initiate a robust response to Rift Valley fever virus infection and identified a key immune pathway that is critical for the ability of microglia to respond to infection. When this immune pathway is rendered non-functional, mice have a dysregulated response to infection in the brain. This study provides insight into how the immune response can control Rift Valley fever virus infection of the brain.

Introduction

Rift Valley fever virus (RVFV) (genus *Phlebovirus/*family *Bunyaviridae*), is a highly pathogenic mosquito-borne virus that can cause lethal disease in both humans and livestock, including acute-onset hepatitis, delayed-onset encephalitis, blindness, or hemorrhagic fever [1]. RVFV is endemic to Africa however concern exists about its potential spread across the world, similar to Zika or West Nile virus (WNV) [1]. Outside of Africa, competent vectors for RVFV include over 30 species of mosquitoes that are present throughout North and South America [2]. RVFV is also classified as a Category A Biodefense pathogen by the National Institute of Allergy and Infectious Diseases (NIAID) due to the potential for intentional spread by aerosol and the lack of licensed vaccines or antiviral therapeutics. Furthermore, RVFV is classified by the Department of Health and Human Services (HHS) and United States Department of Agriculture (USDA) as an overlap select agent due to the susceptibility of numerous livestock species to this disease [3].

68   In the event of an intentional release, the most likely route of exposure to RVFV would be
69   through the respiratory system via aerosolized release of the virus. Studies conducted using
70   rodent models indicate a more severe infection following respiratory versus subcutaneous
71   exposure, with higher incidence of lethality, neuropathology, and increased viral titers in the
72   brain [4-7]. Analysis of human infections also suggests that aerosol exposure to RVFV (i.e.,
73   laboratory acquired infections and infections acquired via handling of infected livestock) leads to
74   a higher incidence of severe disease with encephalitis and long-lasting neurologic complications
75   [8, 9]. The fatality rate amongst patients with encephalitic manifestations of disease is ~50%
76   [10], which is much higher than the overall fatality rate, estimated to be between 0.5-2% [11].
77   Thus, a thorough understanding of RVFV pathogenesis in the brain is required for preparedness
78   to combat the virus' worst outcomes, including intentional release of the virus.
79
80   The term "immune privileged site" was once applied to the brain and interpreted to mean that
81   few immune defenses were functional in this organ [12]. However, it is now widely accepted that
82   the brain is highly immunologically active [13]. An emerging body of evidence indicates that
83   immune responses within the brain are critical for control of an array of neuroinvasive viruses
84   [14, 15]. In the brain, neurons, and glial cells (e.g., astrocytes, and microglia), express many of
85   the same pattern recognition receptors (PRRs) expressed by cells in the periphery and initiate
86   type I interferon (IFN) expression as well as other innate responses upon viral infection [15, 16].
87   Such early responses in the brain are critical for direct control of viral replication, as well as for
88   recruitment of adaptive immune cells that participate in viral clearance [17, 18]. Microglia, the
89   resident immune cells of the brain, play a key role in bridging innate and adaptive immune
90   responses in the brain [19-21], and depletion of microglia increases susceptibility to multiple
91   viral infections [18, 22, 23]. Although potent immune responses are required for viral control in
92   the brain, limiting inflammation presents a unique immunoregulatory challenge as excessive
93   inflammation can be especially deleterious and promote neurodegenerative diseases such as
94   Parkinson's [24] and Alzheimer's [25] disease. Thus, investigation of immune responses in the
95   brain presents an opportunity to understand the interaction of processes that hone the correct
96   response to control viral replication without inducing excessive damaging inflammation.
97
98   To date, there has been limited investigation of the immune response to RVFV in the brain.
99   Previous work has indicated that a strong adaptive response involving both CD4 and CD8 T cells
100   as well as a robust antibody response is required for the prevention of encephalitic disease [7, 26,
101   27] yet there remains a lack of understanding of the response of resident and infiltrating immune
102   cells in the brain. Furthermore, the PRRs that microglia use to respond to RVFV infection have
103   not yet been identified. Previous work has demonstrated the critical role of RIG-I-like receptor
104   (RLR) signaling *via* mitochondrial antiviral signaling (MAVS) in the type I IFN response of
105   macrophages and dendritic cells (DCs) to RVFV infection, as well as a protective role for MAVS
106   following *in vivo* challenge, with little to no contribution from the RNA-sensing toll-like
107   receptors (TLRs) [6]. However, differential roles for the RNA-sensing PRRs during viral
108   infections of the CNS have been identified, most notably for WNV, where TLR3, TLR7, and
109   RLR receptors RIG-I and MDA-5 have been shown to coordinate and propagate a protective
110   response [28-30]. Identifying the relative contributions of innate signaling pathways to the
111   induction of type I IFNs and subsequent control of viral infection has important consequences in
112   terms of understanding human susceptibility to RVFV infection, as polymorphisms in TLR3,

113   TLR7, their respective downstream signaling adaptors TRIF and MyD88, as well as RIG-I and
114   MAVS have all been associated with severe disease/neuropathology in humans [31].
115
116   Here, we investigated the immune response in the murine brain to RVFV intranasal infection.
117   We demonstrate that microglia mount a robust response that is dependent on MAVS and
118   independent of TLR3 and TLR7. MAVS is critical for the expression of immunoregulatory
119   genes, secretion of cytokines, and upregulation of surface markers of activation. *Mavs*$^{-/-}$ mice are
120   more susceptible to infection, with higher viral titers in the brain following intranasal challenge.
121   RNA sequence (RNA-seq) analysis of whole brain tissue revealed robust immune gene
122   expression with greater induction of inflammatory genes in the brains of *Mavs*$^{-/-}$ versus wild type
123   (WT) mice. Single cell RNA-sequence (scRNA-seq) analysis revealed defects in specific
124   antiviral genes and signaling pathways within microglia in the brains of RVFV infected *Mavs*$^{-/-}$
125   mice. The lack of MAVS resulted in a shift towards a more inflammatory phenotype, with a
126   decrease in antiviral signaling pathways and an increase in proinflammatory pathways within
127   *Mavs*$^{-/-}$ microglia. Differences in immune infiltration into the brain were also observed between
128   WT and *Mavs*$^{-/-}$ mice. These results are an important step towards understanding the cell types
129   and molecular pathways responsible for controlling RVFV infection in the brain and towards
130   future developments of antiviral treatments.
131
132   **Results**
133
134   *RVFV infection induces a robust response in microglia that is dependent upon Mavs and*
135   *independent of Tlr3 and Tlr7*
136
137   To determine if microglia respond to RVFV infection directly *via* cell intrinsic mechanisms, we
138   first confirmed infection of microglia cell lines EOC 13.31 and SIM A9, as well as primary
139   microglia derived from the brains of neonatal mice *via* flow cytometry using a RVFV-specific
140   antibody (Figure 1A and B). Vero cells were also included as a positive control for infection.
141   EOC 13.31 cells had the lowest infectivity rate ranging from 30-40% positive cells, while
142   primary microglia displayed infectivity rates (50-70%) similar to SIM A9 cells (60-70%) but
143   slightly less effective than the Vero positive control (90%) (Figure 1B). Both the fully virulent
144   (ZH501) and attenuated (MP-12) strains of RVFV yielded similar levels of infected primary
145   microglia (Figure 1C). Next, we probed the response of primary microglia to both the ZH501
146   and MP-12 strains by quantifying changes in expression of genes involved in antiviral immune
147   responses using real-time reverse transcription (RT^2) PCR array (Figure 1D and Table S1). There
148   was a significant response to both viruses with similar patterns of gene expression changes,
149   although the overall magnitude of the response was greater in microglia infected with the
150   attenuated versus the fully virulent strain, consistent with prior reports [32]. The response to MP-
151   12 was robust, with very high levels of *Ifnb1* expression (greater than 7,000-fold upregulation)
152   and greater than 10-fold upregulation of over 20 genes, including *Ifna2, Ifih1, Isg15, Cxcl10, Il6,*
153   and *Il12b,* among others.
154
155   Next, microglia derived from WT, *Tlr3*$^{-/-}$*, Tlr7*$^{-/-}$*,* or *Mavs*$^{-/-}$ mice were infected with MP-12, and
156   a similar infectivity rate was confirmed amongst all groups, therefore was independent of
157   genotype (Figure S1). Microglia derived from TLR3 or TLR7 deficient animals activated
158   immune genes in response to RVFV at levels similar to WT microglia (Figure 2A and B and

159   Table S1). In contrast, microglia derived from *Mavs*^{-/-} mice displayed an abrogated response to
160   infection, with minimal changes in gene expression in most genes in the array and a greater than
161   4,000-fold reduction in *Ifnb1* expression versus WT infected microglia (Figure 2C and Table
162   S1).
163
164   We further characterized the role of MAVS in the response of microglia to RVFV infection *in*
165   *vitro* by assessing expression of microglial activation markers as well as cytokine secretion
166   (Figure 3). Microglia upregulated surface expression of CD86, CD80, and I-A/I-E in a MAVS-
167   dependent manner (Figure 3A). Using RVFV antibody staining, cells within infected cultures
168   could be identified as infected (RVFV[+]) or uninfected (RVFV[-]). Expression was upregulated not
169   only on infected microglia (RVFV[+]), but also on uninfected cells within the culture (RVFV[-]),
170   suggesting secreted cytokines can influence the activation state of cells in trans. Within WT
171   microglia, expression of each marker was highest on infected cells, with an intermediate level of
172   expression seen on cells activated in trans. On *Mavs*^{-/-} microglia, apart from a low level of CD80
173   on infected cells, no significant upregulation of activation markers was observed. In contrast,
174   upregulation of activation markers was unaltered from WT on *Tlr3*^{-/-} and *Tlr7*^{-/-} microglia (Figure
175   S2).
176
177   Cytokine secretion by infected microglia was also dependent on MAVS (Figure 3B). High levels
178   of type I IFNs were detected in supernatants from WT infected cells, as well the inflammatory
179   cytokines IL-6 and TNF-α, and chemokines CCL5, CXCL10, CXCL11, and CCL2. Cytokine
180   levels in supernatants from MAVS-deficient cells were either not detectable, or not significantly
181   different from uninfected supernatants. Taken together, these data demonstrate that microglia
182   have a robust response to RVFV infection that is mediated primarily through the RLR signaling
183   adaptor MAVS.
184
185   *Mavs*^{-/-} *animals have a dysregulated immune response with increased susceptibility to infection*
186
187   We then investigated the role of MAVS in the immune response in the brain during *in vivo*
188   challenge with RVFV (Figure 4). Intranasal challenge of WT and *Mavs*^{-/-} cohorts of mice (n=20)
189   with the ZH501 strain of RVFV confirmed enhanced susceptibility to infection of *Mavs*^{-/-} mice,
190   consistent with prior reports [6]. *Mavs*^{-/-} mice succumbed to challenge significantly faster, with
191   100% of *Mavs*^{-/-} mice deceased by 6 days post infection, whereas 20% of WT animals were still
192   alive 10 days post infection (Figure 4A). To capture early innate antiviral responses, we
193   conducted a longitudinal study over 4 days, where infected brains of WT mice were examined *ex*
194   *vivo* to determine when live virus (MP-12) could be cultured from brain tissue following
195   intranasal challenge (Figure S3). Day 7 post-infection was identified as the earliest timepoint live
196   virus could be detected in infected WT brains. Next, we compared viral levels at day 7 post
197   infection with MP-12 between WT and *Mavs*^{-/-} mice and were able to detect infection in 100% of
198   *Mavs*^{-/-} (n=11), but only in 42% of WT (n=12) infected brains. Within brains with detectable
199   virus, titers of live virus as well as the levels of RVFV genomic RNA were significantly higher
200   in *Mavs*^{-/-} than in WT mice (Figure 4B).
201
202   To assess the antiviral response, we utilized RNA-seq to profile the transcriptomic alterations
203   induced by RVFV infection in the brains of WT and *Mavs*^{-/-} mice. Infection resulted in
204   significant upregulation of 1,069 genes in the brains of WT mice and 1,116 genes in the brains of

205   *Mavs*-/- mice where 600 upregulated genes were in common to both WT and *Mavs*-/- (Figure 4C
206   and Table S2). Downregulation of genes in response to infection displayed less overlap between
207   WT and *Mavs*-/-, with 977 downregulated in WT, 729 downregulated in *Mavs*-/-, and only 165
208   downregulated genes common to both genotypes (Figure 4C). Functional enrichment of
209   differentially expressed genes revealed strong correlation of pathways related to innate immune
210   and defense responses in both WT and *Mavs*-/- brains, including response to other organism
211   (GO:0051707), innate immune response (GO:0045087), response to cytokine (GO:0034097),
212   and cytokine production (GO:0001816) (Figure 4D).
213
214   To identify deficiencies in the antiviral response within *Mavs*-/- brains that would indicate the
215   effector functions downstream of MAVS signaling that control viral replication, we focused on
216   pathways that were enriched in WT and unaffected in *Mavs*-/- infected brains. Interestingly, only
217   two pathways were enriched in WT and not *Mavs*-/- yet neither are involved in immune responses
218   nor indicate any functional advantage WT animals have at controlling viral replication (Figure
219   4D). *Mavs*-/- brains had more exclusively enriched pathways, including regulation of cytokine
220   production (GO:0001817) and inflammatory response (GO:0006954), indicating that the overall
221   levels of inflammation were higher in *Mavs*-/- brains than in WT. This is consistent with previous
222   reports that indicated a more robust serum cytokine response in *Mavs*-/- than WT mice infected
223   with RVFV [6].
224
225   IFN α/β gene expression levels were elevated in WT infected brains, whereas induction was not
226   seen in *Mavs*-/- brains (Figure 4E). However, global upregulation of type I interferon signaling
227   was not observed in the whole brain between WT and *Mavs*-/-. Thus, while a deficiency in type I
228   interferons is noted in *Mavs*-/- brains, examination of downstream signaling does not reveal
229   potential deficiencies in antiviral response genes. In total, the data demonstrate that RVFV
230   infection results in robust activation of immune and inflammatory genes in both WT and *Mavs*-/-
231   brains with very similar patterns of gene upregulation in both.
232
233   *Single cell RNA sequencing reveals changes in immune infiltration and signaling defects in*
234   *microglia following RVFV infection of Mavs*-/- *mice*
235
236   Next, we performed scRNA-seq to increase the resolution of transcriptional analysis and assess
237   cellular variations resulting from the absence of MAVS during RVFV infection of the brain.
238   Single cell suspensions were generated from whole brain tissue of WT and *Mavs*-/- mice, with
239   (WT+, *Mavs*-/-+) and without (WT-, *Mavs*-/--) RVFV infection. The following cell numbers were
240   sequenced from each condition: WT-: 1,989, *Mavs*-/--: 1,749, WT+: 1627, *Mavs*-/--: 1841, for a
241   total of 7,206 cells. Unsupervised clustering of the data resulted in 15 cell type clusters (Figure
242   5A). By cross-referencing genes differentially expressed in each cluster to previously published
243   cell-type specific markers [33-36], we assigned each cluster to its putative cell-type identity
244   (Figure 5C). We identified expected cell clusters such as neurons, astrocytes, oligodendrocytes,
245   and endothelial cells. Three clusters of immune cells were identified, corresponding to
246   microglia/myeloid cells, T/natural killer (NK) cells, and neutrophils. We observed a large shift in
247   the relative frequency of immune cells upon infection, indicating massive immune infiltration in
248   the brains of infected animals (Figure 5B and D). Sequenced cells from uninfected brains were
249   comprised of 70-80% non-immune cells (clusters 1, 2, 4-9, and 11), with immune cells (clusters
250   0, 3 and 10) comprising less than 30%. In contrast, sequenced cells from infected brains were

251 comprised of 30-40% non-immune and more than 60% immune cells (Figure 5B and D).
252 Interestingly, the pattern of immune infiltration differed between WT and *Mavs*^{-/-} infected brains.
253 WT animals exhibited infiltration of mostly myeloid lineage cells, whereas *Mavs*^{-/-} animals
254 exhibited infiltration of lymphocyte populations in addition to myeloid lineage cells (Figure 5D).
255 Immune infiltration was confirmed using flow cytometry (Figure 5 E-G) and was consistent with
256 scRNA-seq ratios. Lymphocytes and non-glial cells of myeloid lineage comprised a very small
257 fraction of immune cells within uninfected brains, ranging from 0.5-4% and 1-6% of brain
258 immune cells, respectively (Figure 5F and G). In contrast, the percentage of non-glial myeloid
259 cells increased to 10-25% of brain immune cells in both WT and *Mavs*^{-/-} infected mice (Figure
260 5F). Lymphocytes also increased in the brains of both WT and *Mavs*^{-/-} infected mice, however
261 significantly more lymphocytes were observed in the brains of *Mavs*^{-/-} mice (Figure 5G), with
262 lymphocytes comprising 5-15% of brain immune cells in WT mice and 15-30% of brain immune
263 cells in *Mavs*^{-/-} mice.
264
265 Clustering of microglia/myeloid cells (cluster 0, Figure 5A) identified 6 subclusters of myeloid
266 cells (Figure 6A). Enumeration of cells according to condition suggested that most immune cells
267 present in uninfected brains were microglia, whereas infected brains contained cells of multiple
268 infiltrating lineages including monocytes, antigen presenting cells (APCs), and granulocytic cells
269 (Figure 6B and D). The distribution of myeloid lineage cells in uninfected brains confirmed the
270 flow cytometry data in Figure 5E and is consistent with previously published reports [37] which
271 indicate that microglia are the predominant immune cell type in the brain under non-pathological
272 conditions. The relative frequency of macrophages (cluster 4) was consistent across conditions
273 and likely corresponds to resident non-parenchymal macrophages [38], rather than an infiltrated
274 population. Infected brains of both genotypes demonstrated similar patterns of monocyte, APC,
275 and granulocytic cell infiltration (clusters 2, 3, and 5, respectively). Overall, the distribution of
276 myeloid cells was similar between infected brains of both genotypes.
277
278 Next, we examined transcriptional differences in the antiviral responses of microglia derived
279 from WT and *Mavs*^{-/-} infected brains. Differences in type I IFN (*Ifnb1* and *Ifna2*) expression
280 were noted in a subset of microglia in WT infected brains whereas levels were undetectable in
281 microglia from *Mavs*^{-/-} infected and uninfected brains of both genotypes (Figure 6E). Gene
282 ontological analysis revealed specific enrichment of pathways involved in antiviral responses
283 including response to virus (GO:009615), negative regulation of viral genome replication
284 (GO:0045071), antigen processing and presentation (GO:0019882), and response to type I
285 interferon (GO:0034340) within WT infected microglia (Figure 6F). In contrast, inflammatory
286 pathways such as response to interleukin-1 (GO:007055) and positive regulation of interleukin-6
287 production (GO:0032755), as well as pathways involved in cell migration such as regulation of
288 chemokine production (GO:0032642) and positive regulation of cell adhesion (GO:0045785)
289 were enriched in *Mavs*^{-/-} microglia (Figure 6G). Specific IFN-stimulated genes (ISGs) were
290 expressed at higher levels within WT microglia, including *Irf7, Isg20, Isg15, Oasl1, Ifit1, Ifit3,*
291 *Ifi27l2a,* and *Bst2* (Figure 6H). Genes that have been previously associated with a pro-
292 inflammatory state [39-41] were expressed at higher levels within *Mavs*^{-/-} microglia, including
293 *Irf1, Irf8, Il1b,* and *Nos2* (Figure 6H).
294
295 Flow cytometric analysis revealed further defects in *Mavs*^{-/-} microglia. In line with increased
296 viral titers in the brains of *Mavs*^{-/-} animals (Figure 4B), microglia from *Mavs*^{-/-} animals displayed

297 dramatically higher levels of infection as evidenced by anti-RVFV antibody staining, ranging
298 from 0.5-9% in WT brains to 15-50% in *Mavs*$^{-/-}$ brains (Figure 6I). We also evaluated the surface
299 expression levels of activation markers; expression of CD86 mirrored *in vitro* results, with WT
300 microglia that are RVFV$^+$ expressing the highest levels of CD86, and microglia from infected
301 brains that are RVFV$^-$ expressing an intermediate level of CD86, although not significantly
302 different from microglia from uninfected brains (Figure 6J). There was no significant
303 upregulation of CD86 on microglia from *Mavs*$^{-/-}$ brains. Expression of I-A/I-E was also elevated
304 on RVFV$^+$ microglia, although not on RVFV$^-$ microglia, from WT infected brains (Figure 6K).
305 In contrast to *in vitro* results, upregulation of I-A/I-E was detected on microglia derived from
306 *Mavs*$^{-/-}$ brains (Figure 6K). No significant upregulation of CD80 was detected (Figure S4).
307
308 *Lymphocyte infiltration and signaling defects in the brains of Mavs*$^{-/-}$ *mice*
309
310 The majority of lymphocytes identified within WT infected brains were NK cells, whereas those
311 in *Mavs*$^{-/-}$ infected brains included a large number of T cells in addition to NK cells (Figure 7A-
312 D). Lymphocytes comprised greater than 30% of the total sequenced cells in the *Mavs*$^{-/-}$ infected
313 condition (Figures 5D and 7D). Upon examining genes that were differentially expressed
314 between WT and *Mavs*$^{-/-}$ lymphocytes, we observed defects in ISG expression (*Irf7, Ifi44, Xcl1*),
315 as well as genes involved in T and NK cell-mediated killing (*Prf1, Gzmb, Ifng*) [42] within
316 lymphocytes from *Mavs*$^{-/-}$ infected animals (Figure 7E), suggesting that *Mavs*$^{-/-}$ cells are less
317 efficient in clearing the virus than WT cells [43-45]. Consistent with this, we observed reduced
318 expression of *Il15*, *Il18,* and *Il27*, cytokines that have a stimulatory effect on T and NK cells [46-
319 49], in microglia from infected *Mavs*$^{-/-}$ mice (Figure S5). Lower levels of IFN-γ protein were also
320 detected in the brains of *Mavs*$^{-/-}$ versus WT infected mice (Figure 7G). Taken together, these
321 results suggest that a defective response of *Mavs*$^{-/-}$ microglia may lead to the reduced capacity of
322 T and NK cells to control RVFV infection.
323
324 **Discussion**
325
326 Despite the major role of pathogenesis in the brain for the most severe outcomes of RVFV
327 infection, there has been little investigation of local antiviral immune responses within this
328 organ. Here, we investigated the innate immune response in the brain to RVFV in a mouse model
329 of intranasal infection. We demonstrated that microglia mount a robust response to RVFV that is
330 dependent on MAVS and independent of TLR3 and TLR7. To probe viral pathogenesis in the
331 brain in the presence and absence of a functional innate immune response, we profiled the brains
332 of WT and *Mavs*$^{-/-}$ animals following intranasal infection with RVFV. *Mavs*$^{-/-}$ animals
333 succumbed to infection more rapidly and with significantly higher viral titers in the brain. Viral
334 presence in the brain corresponded with massive immune infiltration in both WT and *Mavs*$^{-/-}$
335 mice, consisting mostly of myeloid lineage cells as well as some lymphocytes, with significantly
336 more T and NK cells in the brains of *Mavs*$^{-/-}$ animals. Robust immune gene expression was
337 observed in the brains of both WT and *Mavs*$^{-/-}$ infected animals, with greater inflammatory gene
338 expression within *Mavs*$^{-/-}$ brains. Deficiencies in type I IFN expression were noted within whole
339 brain tissue as well as specifically within microglia in *Mavs*$^{-/-}$ infected animals, and furthermore,
340 microglia from *Mavs*$^{-/-}$ animals displayed deficiencies in downstream antiviral signaling
341 pathways and specific ISG expression. T and NK cells from *Mavs*$^{-/-}$ animals were also deficient

342   in ISG expression, as well as genes related to killing functions. Furthermore, decreased *Ifng*
343   expression resulted in lower levels of IFN-γ protein in the brain.
344
345   A summary of previous studies using mouse models of infection suggests that failure to establish
346   a robust peripheral immune response to RVFV infection allows for viral spread to the brain, and
347   exposure via the respiratory route increases the likelihood of bypassing such a protective
348   response [4, 5, 26, 27, 50]. Thus, these studies suggest that the primary function of a protective
349   response is to prevent the virus from ever reaching the brain. However, a recent study using a rat
350   model of infection provided additional insight into the role of immune responses within the
351   brain. Albe *et. al* [7] observed that rats infected subcutaneously with RVFV had detectable viral
352   RNA in the brain as early as one day post infection despite lacking overt signs of disease.
353   Furthermore, T cell infiltration into the brain was associated survival of infection, suggesting that
354   functional T cell responses in the brain are ultimately capable of clearing infection and
355   promoting survival and recovery. Rats exposed to aerosolized RVFV did not display T cell
356   infiltration in the brain, and ultimately succumbed to infection. This study is consistent with the
357   hypothesis that the lack of a robust peripheral immune response leads to increased pathogenesis
358   within the brain, however it suggests that extension of peripheral responses to the brain is critical
359   for the resolution of RVFV infection. Our present work indicates that innate immune responses
360   to RVFV are robustly active within the brain. Thus, the role that cells within the brain play in
361   recruiting and orchestrating a protective response warrants further investigation.
362
363   Microglia express a number of PRRs and respond to a wide variety of infectious agents in a
364   diverse manner and can alternately establish an anti- or pro-inflammatory environment,
365   depending on the specific genes that are induced as well as differing factors in the surrounding
366   environment [51, 52]. Our results indicate that RVFV readily infects microglia, which then
367   primarily utilize the RLR pathway via the signaling adaptor MAVS to detect and respond to
368   RVFV infection. *In vitro*, microglia derived from *Mavs*$^{-/-}$ animals displayed abrogated antiviral
369   responses including diminished type I IFN and IFN-responsive gene expression and diminished
370   capacity to upregulate surface markers of activation or secrete cytokines. Despite being severely
371   attenuated, some response to infection was still noted, therefore we cannot rule out a minor role
372   for other receptor(s) in the response of microglia to RVFV infection. Evaluation *in vivo* within
373   *Tlr3*$^{-/-}$ or *Tlr7*$^{-/-}$ mice may reveal a role for these receptors, which might vary in importance
374   within specific cell and tissue types.
375
376   The response of microglia to RVFV infection *in vivo* was also dependent on MAVS. Using
377   scRNA-seq, we demonstrated that microglia in WT infected brains express type I IFNs and
378   interferon responsive genes. Pathways that were enriched in WT microglia versus *Mavs*$^{-/-}$
379   included response to virus and negative regulation of viral genome replication, indicating that
380   WT microglia have a greater capacity to control viral infection. Specific ISGs with demonstrated
381   antiviral activity were elevated including *Ifit1* and *Ifit3,* both of which have previously been
382   shown to bind RVFV genomic RNA and have inhibitory activity on viral growth [53]. BST-2 has
383   previously been shown to inhibit replication of several viruses, including HIV-1 and Lassa Virus,
384   but was not capable of inhibiting RVFV replication in the cell types tested [54, 55]. Further
385   investigation is required to determine if these ISGs have anti-RVFV activity in microglia. Other
386   ISGs that were among the 20 most upregulated genes in WT microglia include master regulatory
387   genes *Irf7* and *Isg15*, broad spectrum exonucluease *Isg20, Ifi27l2a,* which has been shown to

388   have antiviral activity against WNV [56], and *Oasl1*, which can regulate *Irf7* expression [57].
389   Using flow cytometry, we demonstrated that WT microglia upregulate CD86 and I-A/I-E on the
390   cell surface in response to RVFV infection. Upregulation of surface markers was restricted to
391   microglia that were RVFV$^+$, which were of relatively low abundance in WT brains. Separating
392   microglia from infected brains into RVFV$^+$ and RVFV$^-$ populations was restricted to antibody
393   staining and was not possible using scRNA-seq due to the sequencing technology being unable
394   to capture RVFV genomic RNA. While we cannot ascertain which sequenced microglia were
395   infected or uninfected, it can be inferred that the changes in gene expression observed within WT
396   microglia were induced largely in trans in response to secreted factors from neighboring cells
397   due to the low levels of infection detected by antibody staining.
398
399   In contrast, microglia from *Mavs*$^{-/-}$ brains displayed much higher levels of infection, ranging
400   from 15-50% of the total microglia. *Mavs*$^{-/-}$ microglia did not express type I IFNs, and
401   upregulated genes enriched in inflammatory processes such as response to interleukin-1 and
402   positive regulation of interleukin-6. *Mavs*$^{-/-}$ microglia upregulated surface expression of I-A/I-E,
403   on both RVFV$^+$ and RVFV$^-$ microglia *in vivo*. Antigen processing and presentation was observed
404   transcriptionally only within WT microglia, therefore the functional significance of I-A/I-E
405   expression is unclear. Interestingly, *Irf1*, *Irf8*, and *Il1b* were amongst the genes most upregulated
406   in *Mavs*$^{-/-}$ microglia versus WT. Previous studies utilizing a mouse model of nerve injury
407   indicated increased *Il1b* expression by microglia that was dependent on *Irf1* and *Irf8* expression
408   [39, 40]. These studies in conjunction with our present study suggest that different types of
409   pathological insults can activate a common inflammatory state in microglia and further suggest
410   that failure to establish an appropriate antiviral response may dispose the microglia to remain in
411   a proinflammatory state.
412
413   Our results highlight the importance of MAVS in orchestrating a protective immune response
414   against RVFV infection in the brain. The lack of MAVS resulted in a dysregulated immune
415   response, with more inflammatory gene expression and less functional adaptive immune
416   responses. The brain infiltrating lymphocytes consisted of T and NK cells in both WT and *Mavs*$^-$
417    $^{/-}$ animals however more NK than T cells were observed in WT. Furthermore, the T and NK cells
418   in the brains of *Mavs*$^{-/-}$ mice appear to be functionally deficient due to decreased expression of
419   ISGs and genes related to killing functions. Thus, while more cells are recruited to the brain,
420   likely due to the increased presence of viral antigen, they are less able to control viral replication.
421   This is in line with previous studies investigating the role of MAVS in WNV infection which
422   demonstrated increased infiltration of T cells with lower functional avidity into the brains of
423   *Mavs*$^{-/-}$ mice [30, 58]. Further work is needed to characterize the functional deficiency of T cells
424   in *Mavs*$^{-/-}$ mice during RVFV infection and to understand the molecular details that govern this
425   deficiency. Moreover, the role of NK cells in RVFV infection has not been investigated, and our
426   data suggests that NK cells may be actively recruited to the brain to help control RVFV
427   infection. Interestingly, we observed increased expression of *l15*, *Il18*, and *Il27*, which have been
428   shown to activate T and NK cells [46-49], in WT microglia and other myeloid cells. Secretion of
429   these cytokines may be one mechanism by which microglia regulate the cytotoxic activity of
430   lymphocytes, and lack of expression in *Mavs*$^{-/-}$ microglia could be playing a role in the defective
431   lymphocyte responses observed in these animals. Future studies will explore the relationship
432   between secreted factors from microglia and the induction of protective T and NK cell responses
433   during RVFV infection of the brain. Taken together, previous studies and our present study

434 indicate that RLR signaling through MAVS is required not only to control viral replication early
435 but is also necessary to induce a fully functional adaptive response.
436
437 In summary, this present work provides a better understanding of the immune response in the
438 brain to RVFV infection. Furthermore, it defines a protective role for MAVS in propagating
439 antiviral responses in the brain and suggests that signaling through MAVS may also be required
440 for functional T and NK cell responses in the brain. Better understanding of the immune
441 responses that are active against RVFV in the brain may contribute to therapeutics that
442 effectively harness or augment these responses and lead to treatments for encephalitic disease.
443
444 **Materials and Methods**
445
446 **Cells and viruses**
447 Vero, EOC 13.31, SIM A9, and LADMAC cells were obtained from the American Type Culture
448 Collection (ATCC). Cell lines were maintained in the following culture media: Vero: Dulbecco's
449 modified Eagle's medium (DMEM) supplemented with 10% fetal bovine serum (FBS). EOC
450 13.31: DMEM supplemented with 10% FBS and 20% LADMAC conditioned media to provide a
451 source of CSF-1 to support microglial growth [59]. SIM-A9: DMEM:F12 supplemented with
452 10% FBS and 5% horse serum. LADMAC: Minimal essential medium supplemented with 10%
453 FBS. Primary glial cells: RPMI 1640 supplemented with 10% FBS and 0.01 mg/mL gentamicin
454 and 0.25 μg/mL amphotericin. All media was supplemented with 100 units/ml penicillin and 100
455 μg/ml streptomycin, and all cells were maintained at 37 °C in 5% CO2. All cell culture reagents
456 were obtained from Thermo Fisher. LADMAC conditioned media was prepared by collecting
457 supernatant from confluent cells that have been in culture for 5-7 days and centrifuged at 300 x g
458 for 10 min to remove cellular debris.
459
460 Wild type Rift Valley fever virus (RVFV) strain ZH-501 was obtained from the NIH Biodefense
461 and Emerging Infections Research Resources Repository, NIAID, NIH. The MP-12 strain was
462 kindly provided by Oscar Negrete (Sandia National Laboratory). RVFV stocks were propagated
463 in Vero cells as previously described [60, 61]. Titers of viral stocks were determined by standard
464 plaque assay consisting of an agarose overlay and crystal violet staining. All work with the
465 ZH501 strain was performed in Institutional Biosafety Committee approved BSL-3 and ABSL-3
466 facilities at Lawrence Livermore National Laboratory using appropriate PPE and protective
467 measures.
468
469 **Mice**
470
471 All animal work was conducted in accordance with protocols approved by the Lawrence
472 Livermore National Laboratory Institutional Animal Care and Use Committee. C57BL/6 as well
473 as mice genetically deficient in MAVS *(B6;129-Mavs^{tm1Zjc}/J*; Jax stock No: 008634*)*, TLR3
474 B6;129S1-*Tlr3^{tm1Flv}*/J; Jax Stock No: 005217*)*, and TLR7 (B6.129S1-*Tlr7^{tm1Flv}*/J; Jax stock No:
475 008380) were obtained from Jackson Laboratory. For experiments using knockout (KO) mice,
476 animals were crossed to WT C57BL/6 mice to generate a heterozygous F1 generation. F1
477 littermates were crossed to generate homozygous WT and KO F2 progeny. Matched WT and KO
478 animals from the same generation were used for each genotype. All animals were maintained in
479 PHS-assured facilities.

480

Isolation of primary microglia isolation

482

Primary microglia were isolated and cultured as described previously [62, 63]. Briefly, brains from 1 – 4-day old neonatal mice were dissected to remove meninges and large blood vessels and finely minced with sterile surgical scissors. The minced tissue was then forced through a 70 μM cell strainer (Fischer Scientific) and rinsed with cold glial media. Cells were pelleted at 300 x g for 10 min then resuspended in 20 mL fresh media and placed in a T75 flask (1 flask per 7 – 9 brains) and maintained in culture for 2 weeks. Microglia were harvested from the mixed glial culture by shaking flasks for 4 h at 200 rpm using an orbital shaker. Cells were pelleted at 300 x g for 10 min and resuspended in 10 mL microglia growth media (glial media + 20% LADMAC conditioned media). Microglia from up to 3 T75 flasks were combined and placed in a T25 flask. Microglia were maintained in culture for up to one week before use in viral infection experiments.

In vitro **infection of microglia**

496

Microglia were plated in 24 well tissue culture treated plate at a density of 250,000 cells per well primary glial cell media. Cells were infected with RVFV at a MOI of 5 (qPCR analysis) or 2 (flow cytometry/cytokine analysis) in primary glial cell media. Cells were incubated with virus for 4 h at 37 °C in 5% CO2. Viral infection media was then removed, and cells used for qPCR analysis were lysed for RNA extraction. Cells used for flow cytometry and cytokine analysis were washed one time with PBS, then replenished with fresh media and incubated for another 18-24 h. Supernatants were then removed and stored at -80 °C for cytokine analysis, and cells were processed for flow cytometric analysis. Data for all *in vitro* assays is displayed as the average from 3 triplicate wells and is representative of an experiment performed at least twice.

506

Cytokine analysis

508

Cytokines were quantified using Legendplex multiplex bead-based assay (Biolegend) using the mouse anti-virus response panel according to manufacturer's instructions. Flow cytometry of the beads was performed using a FACSAria Fusion and data were analyzed using Biolegend's cloud-based analysis software available at https://legendplex.qognit.com.

513

In vivo **infection**

515

Groups of male and female *Mavs*$^{-/-}$ and wildtype (WT) control littermates ranging in age from 8-12 weeks were inoculated intranasally with 5×10^5 (MP-12, n=12) or 1000 PFU (ZH501, n=20) RVFV while under anesthesia (4-5% isoflurane in 100% oxygen). Mice were monitored daily for signs of morbidity and animals were humanely euthanized upon signs of severe disease by CO_2 asphyxiation. For tissue harvest, animals were euthanized by CO_2 asphyxiation and the whole animal was perfused with 30 mL sterile PBS containing 50,000 U/L sodium heparin *via* the left ventricle.

523

Brain tissue isolation and preparation

525

526   Preparation of brain tissue for flow cytometric, RNA sequencing, cytokine, and viral titer
527   analysis was performed as previously described [64]. Following euthanasia and perfusion, brains
528   were removed and placed in digestion buffer (PBS pH 7.4 (Thermo Fisher) + liberase + DNase I
529   (both from Roche) to a final concentration of 1.6 wunsch/mL and 0.5 mg/mL, respectively) on
530   ice in a 1.5 mL tube. Brains were finely diced into 1-2 mm^3 pieces with small scissors. 3-4 pieces
531   were placed into RNAlater (Qiagen) for gene expression analysis. The remaining tissue was
532   digested at 37 °C for 30 min. EDTA was added to a final concentration of 10 mM to stop the
533   digestion reaction. A cell suspension was generated by gentle pipetting followed by passage
534   through a 70 μm cell strainer. The cell strainer was rinsed with PBS supplemented with 5% FBS
535   to a total volume of 20 mL. Aliquots of this suspension were stored at -80 °C for cytokine and
536   viral titer analysis. The remaining suspension was subjected to Percoll gradient centrifugation to
537   purify mononuclear immune cells for flow cytometric analysis as previously described [64].
538
539   **Flow cytometry**
540
541   Cells were incubated for 30 min on ice in 100 μl Hank's balanced salt solution (Thermo
542   Fisher) + 2% FBS with Fc block (1:100 dilution, clone 2.4G2; BD Biosciences) along with the
543   following antibodies (all from BD Biosciences): CD45 APC-Cy7 (1:500, clone 30-F11), CD11b
544   AF488 (1:500, clone M1/70), CD80 BV421 (1:200, clone 16-1OA1), and CD86 PE-Cy7 (1:500,
545   clone GL1). IA/I-E AF647 (1:500, clone M5/114.15.2; BioLegend). Cells were then fixed and
546   permeabilized using BD Cytofix/Cytoperm (BD Biosciences) according to manufacturer's
547   instructions. Cells were then incubated with an anti-RVFV antibody (kindly provided by Dr.
548   Robert Tesh and the World Reference Center of Emerging Viruses and Arboviruses) at 1:500
549   dilution, followed by goat anti-mouse PE secondary antibody (1:1000, Santa Cruz
550   biotechnology). Flow cytometry was performed using a FACSAria Fusion and data were
551   analyzed using FlowJo software. Microglia, other myeloid lineage, and lymphocytes were
552   resolved using CD45 and CD11b expression, with microglia identified as CD45^{int} CD11b^{int},
553   other myeloid as CD45^{hi} CD11b^{hi}, and lymphocytes as CD45^{hi} CD11b$^-$ as previously described
554   [64].
555
556   **qPCR and bulk RNA seq analyses**
557
558   RVFV genomic RNA was quantified in brain tissue as described previously [5, 26, 65]. To
559   normalize between samples, results were normalized to GAPDH expression. For *in vitro* qPCR
560   analysis of immune gene expression, RNA from infected and uninfected microglia was harvested
561   at 4 h post infection using RNeasy plus kits, and cDNA was generated using RT^2 First Strand
562   Synthesis kit (both from Qiagen) according to manufacturer's instructions. Real-time quantitative
563   RT-PCR analysis of the samples was carried out using the mouse antiviral response RT^2 Profiler
564   PCR array (Qiagen) on a 7900HT Fast Real-Time PCR system (Thermo Fisher) according to
565   manufacturer's instructions. Data were analyzed using Qiagen's online analysis software
566   available at https://geneglobe.qiagen.com/us/analyze. Data are shown as the log$_2$ fold change in
567   gene expression in infected versus uninfected samples.
568
569   For bulk sequencing analysis, RNA was harvested from RNAlater preserved brain tissue using
570   RNeasy Plus kit. Poly(A)+-enriched cDNA libraries were generated using the Illumina TruSeq
571   RNA Library Prep kit v2 (Illumina Inc). The 75 bp single-end reads were sequenced was

572   performed using an Illumina (Illumina Inc) NextSeq 500 instrument. Sequencing data quality
573   was checked using FastQC software. Reads were mapped to the mouse reference genome
574   (mm10) using STAR [66]. Read counts per gene locus were summarized with featureCounts
575   [67]. Then the data was normalized using RUVseq [68] to correct for batch effects and other
576   unwanted variations. Genes differentially expressed between uninfected and infected samples
577   were identified using edgeR [69]. Gene ontology (GO) and pathway enrichment analysis was
578   performed using functional annotation tool ToppGene [70]. Heatmaps were generated using
579   heatmap.2 function in 'gplots' R package.
580
581   **Single cell RNA sequencing**
582
583   Mice were euthanized and perfused as described above. Isolated brain tissues were immediately
584   processed using a modified protocol from [71]. Cortices were dissected in cold Hibernate A
585   medium (BrainBits LLC) and sliced to approximately 0.5 mm before transferred to a 15 mL
586   falcon tube with Hibernate A and B27 medium (HABG) (Thermo Fischer Scientific). Collected
587   tissue samples in 15 mL conical tubes were warmed up to 30°C in a shaking water bath for 8
588   minutes, before the HABG supernatant replaced with activated papain (34 U/mL, Worthington
589   Biochemical Corporation) and the tubes placed back into the shaking water bath for tissue
590   digestion (30°C, 150 rpm) for 30 minutes. Cells were released from the digested tissues by
591   trituration using a fire-polished Pasteur pipette. Released cells were collected in the supernatant
592   and filtered through a 70 mm MACS Smart Strainer (Miltenyi Biotec) into a new 15 mL conical
593   tube. The single cell suspension was layered onto a Optiprep density gradient to separate cells
594   from debris, after centrifugation (800 x g, 15 min, 22°C). The debris fraction was collected, and
595   the gradient material diluted with HAGB before tubes were centrifuged (200 x g, 5 min, 22°C).
596   The supernatant was aspirated, and ACK lysis buffer (Thermo Fisher Scientific) was added to
597   the cell suspension remove any remaining red blood cells (5 min, RT). Hank's balanced salt
598   solution (Thermo Fisher) was added to the cell suspension containing the lysis buffer and tubes
599   were centrifuged (200 x g, 5 min, 22°C). To remove dead cells from the single cell suspension, a
600   Dead cell removal kit (Miltenyi Biotec) was used as directed by the vendor.
601
602   Cell pellets were resuspended in PBS with 0.04% non-acetylated BSA and counted on a
603   Countess II automated cell counter prior to single-cell sequencing preparation using Chromium
604   Single-cell 3′ GEM, Library & Gel Bead Kit v3 (10x Genomics Cat # 1000075) on a 10×
605   Genomics Chromium Controller following manufacturers' protocol. Sequencing data was
606   demultiplexed, quality controlled, and analyzed using Cell Ranger (10x Genomics) and Seurat
607   [72]. The Cell Ranger Single-Cell Software Suite was used to perform sample demultiplexing,
608   barcode processing, and single-cell 3′gene counting. Samples were first demultiplexed and then
609   aligned to the mouse genome (mm10) using "cellranger mkfastq" with default parameters.
610   Unique molecular identifier counts were generated using "cellranger count". Further analysis
611   was performed using Seurat [72]. First, cells with fewer than 500 detected genes per cell and
612   genes that were expressed by fewer than 5 cells were filtered out. After pre-processing, we
613   performed data normalization, scaling, and identified 2000 most variable features. Then, anchors
614   for data integration were identified using the 'Find-IntegrationAnchors' function. Next, these
615   anchors were passed to the 'IntegrateData' function and new integrated matrix with all four
616   datasets were generated. Subsequently, dimensionality reduction, clustering, and visualization

617 were performed in Seurat as described before [73]. Genes differentially expressed between
618 clusters were identified using 'FindMarkers' function implemented in Seurat.
619

Acknowledgements and Funding

621

628

Author Contributions Statement

630

631 D.W., N.H., and F.B. conceived and designed the experiments. D.W., F.B., N.H., A.P., D.L.,
632 K.S., and A.R. conducted all *in vitro* and *in vivo* experiments described and D.W., N.H., F.B.,
633 and A.S. performed the data analysis. D.W., N.H., and G.L. wrote the manuscript. All authors
634 contributed to editing the manuscript and approved the final version.
635

Conflict of Interest Statement

637

638 The authors declare no conflict of interest.
639

References

1. Pepin M, Bouloy M, Bird BH, Kemp A, Paweska J. Rift Valley fever virus(Bunyaviridae: Phlebovirus): an update on pathogenesis, molecular epidemiology, vectors, diagnostics and prevention. Vet Res. 2010;41(6):61. doi: 10.1051/vetres/2010033. PubMed PMID: 21188836; PubMed Central PMCID: PMCPMC2896810.

2. Rolin AI, Berrang-Ford L, Kulkarni MA. The risk of Rift Valley fever virus introduction and establishment in the United States and European Union. Emerg Microbes Infect. 2013;2:e81. doi: 10.1038/emi.2013.81.

3. https://www.selectagents.gov/sat/list.htm.

4. Reed C, Lin K, Wilhelmsen C, Friedrich B, Nalca A, Keeney A, et al. Aerosol Exposure to Rift Valley Fever Virus Causes Earlier and More Severe Neuropathology in the Murine Model, which Has Important Implications for Therapeutic Development. PLOS Neglected Tropical Diseases. 2013;7(4):e2156. doi: 10.1371/journal.pntd.0002156.

5. Dodd KA, McElroy AK, Jones TL, Zaki SR, Nichol ST, Spiropoulou CF. Rift valley Fever virus encephalitis is associated with an ineffective systemic immune response and activated T cell infiltration into the CNS in an immunocompetent mouse model. PLoS Negl Trop Dis. 2014;8(6):e2874. Epub 2014/06/13. doi: 10.1371/journal.pntd.0002874. PubMed PMID: 24922480; PubMed Central PMCID: PMCPMC4055548.

6. Ermler ME, Yerukhim E, Schriewer J, Schattgen S, Traylor Z, Wespiser AR, et al. RNA Helicase Signaling Is Critical for Type I Interferon Production and Protection against Rift Valley Fever Virus during Mucosal Challenge. Journal of Virology. 2013;87(9):4846-60. doi: 10.1128/jvi.01997-12.

7. Albe JR, Boyles DA, Walters AW, Kujawa MR, McMillen CM, Reed DS, et al. Neutrophil and macrophage influx into the central nervous system are inflammatory components of lethal Rift Valley fever encephalitis in rats. PLoS Pathog. 2019;15(6):e1007833. Epub 2019/06/21. doi: 10.1371/journal.ppat.1007833. PubMed PMID: 31220182; PubMed Central PMCID: PMCPMC6605717.

8. Anyangu AS, Gould LH, Sharif SK, Nguku PM, Omolo JO, Mutonga D, et al. Risk Factors for Severe Rift Valley Fever Infection in Kenya, 2007. The American Journal of Tropical Medicine and Hygiene. 2010;83(2 Suppl):14-21. doi: 10.4269/ajtmh.2010.09-0293.

9. LaBeaud AD, Pfeil S, Muiruri S, Dahir S, Sutherland LJ, Traylor Z, et al. Factors Associated with Severe Human Rift Valley Fever in Sangailu, Garissa County, Kenya. PLoS Negl Trop Dis. 2015;9(3):e0003548. doi: 10.1371/journal.pntd.0003548.

10. Madani TA, Al-Mazrou YY, Al-Jeffri MH, Mishkhas AA, Al-Rabeah AM, Turkistani AM, et al. Rift Valley fever epidemic in Saudi Arabia: epidemiological, clinical, and laboratory characteristics. Clin Infect Dis. 2003;37(8):1084-92. Epub 2003/10/03. doi: 10.1086/378747. PubMed PMID: 14523773.

11. Javelle E, Lesueur A, Pommier de Santi V, de Laval F, Lefebvre T, Holweck G, et al. The challenging management of Rift Valley Fever in humans: literature review of the clinical disease and algorithm proposal. Ann Clin Microbiol Antimicrob. 2020;19(1):4-. doi: 10.1186/s12941-020-0346-5. PubMed PMID: 31969141.

12. Rustenhoven J. A privileged brain. Science. 2021;374(6567):548. Epub 20211028. doi: 10.1126/science.abl7122. PubMed PMID: 34709902.

684   13.   Lampron A, Elali A, Rivest S. Innate immunity in the CNS: redefining the relationship
685   between the CNS and Its environment. Neuron. 2013;78(2):214-32. Epub 2013/04/30. doi:
686   10.1016/j.neuron.2013.04.005. PubMed PMID: 23622060.
687   14.   Carty M, Reinert L, Paludan SR, Bowie AG. Innate antiviral signalling in the central
688   nervous system. Trends Immunol. 2014;35(2):79-87. Epub 20131206. doi:
689   10.1016/j.it.2013.10.012. PubMed PMID: 24316012.
690   15.   Singh H, Koury J, Kaul M. Innate Immune Sensing of Viruses and Its Consequences for
691   the Central Nervous System. Viruses. 2021;13(2). Epub 2021/01/28. doi: 10.3390/v13020170.
692   PubMed PMID: 33498715; PubMed Central PMCID: PMCPMC7912342.
693   16.   Denizot M, Neal JW, Gasque P. Encephalitis due to emerging viruses: CNS innate
694   immunity and potential therapeutic targets. The Journal of infection. 2012;65(1):1-16. Epub
695   2012/04/10. doi: 10.1016/j.jinf.2012.03.019. PubMed PMID: 22484271.
696   17.   Drokhlyansky E, Göz Aytürk D, Soh TK, Chrenek R, O'Loughlin E, Madore C, et al. The
697   brain parenchyma has a type I interferon response that can limit virus spread. Proc Natl Acad Sci
698   U S A. 2017;114(1):E95-e104. Epub 2016/12/17. doi: 10.1073/pnas.1618157114. PubMed
699   PMID: 27980033; PubMed Central PMCID: PMCPMC5224383.
700   18.   Moseman EA, Blanchard AC, Nayak D, McGavern DB. T cell engagement of cross-
701   presenting microglia protects the brain from a nasal virus infection. Sci Immunol. 2020;5(48).
702   Epub 2020/06/07. doi: 10.1126/sciimmunol.abb1817. PubMed PMID: 32503876; PubMed
703   Central PMCID: PMCPMC7416530.
704   19.   Sanchez JMS, DePaula-Silva AB, Doty DJ, Hanak TJ, Truong A, Libbey JE, et al. The
705   CSF1R-Microglia Axis Has Protective Host-Specific Roles During Neurotropic Picornavirus
706   Infection. Frontiers in Immunology. 2021;12(3568). doi: 10.3389/fimmu.2021.621090.
707   20.   Funk KE, Klein RS. CSF1R antagonism limits local restimulation of antiviral CD8+ T
708   cells during viral encephalitis. Journal of neuroinflammation. 2019;16(1):22. doi:
709   10.1186/s12974-019-1397-4.
710   21.   Mangale V, Syage AR, Ekiz HA, Skinner DD, Cheng Y, Stone CL, et al. Microglia
711   influence host defense, disease, and repair following murine coronavirus infection of the central
712   nervous system. Glia. 2020;68(11):2345-60. Epub 20200525. doi: 10.1002/glia.23844. PubMed
713   PMID: 32449994; PubMed Central PMCID: PMCPMC7280614.
714   22.   Chhatbar C, Detje CN, Grabski E, Borst K, Spanier J, Ghita L, et al. Type I Interferon
715   Receptor Signaling of Neurons and Astrocytes Regulates Microglia Activation during Viral
716   Encephalitis. Cell Rep. 2018;25(1):118-29.e4. Epub 2018/10/04. doi:
717   10.1016/j.celrep.2018.09.003. PubMed PMID: 30282022; PubMed Central PMCID:
718   PMCPMC7103936.
719   23.   Tsai TT, Chen CL, Lin YS, Chang CP, Tsai CC, Cheng YL, et al. Microglia retard
720   dengue virus-induced acute viral encephalitis. Sci Rep. 2016;6:27670. Epub 20160609. doi:
721   10.1038/srep27670. PubMed PMID: 27279150; PubMed Central PMCID: PMCPMC4899773.
722   24.   Tansey MG, Goldberg MS. Neuroinflammation in Parkinson's disease: its role in
723   neuronal death and implications for therapeutic intervention. Neurobiol Dis. 2010;37(3):510-8.
724   Epub 20091110. doi: 10.1016/j.nbd.2009.11.004. PubMed PMID: 19913097; PubMed Central
725   PMCID: PMCPMC2823829.
726   25.   Zhang G, Wang Z, Hu H, Zhao M, Sun L. Microglia in Alzheimer's Disease: A Target for
727   Therapeutic Intervention. Front Cell Neurosci. 2021;15:749587. Epub 20211124. doi:
728   10.3389/fncel.2021.749587. PubMed PMID: 34899188; PubMed Central PMCID:
729   PMCPMC8651709.

730   26.   Dodd KA, McElroy AK, Jones ME, Nichol ST, Spiropoulou CF. Rift Valley fever virus
731   clearance and protection from neurologic disease are dependent on CD4+ T cell and virus-
732   specific antibody responses. J Virol. 2013;87(11):6161-71. Epub 20130327. doi:
733   10.1128/jvi.00337-13. PubMed PMID: 23536675; PubMed Central PMCID: PMCPMC3648110.
734   27.   Harmon JR, Spengler JR, Coleman-McCray JD, Nichol ST, Spiropoulou CF, McElroy
735   AK. CD4 T Cells, CD8 T Cells, and Monocytes Coordinate To Prevent Rift Valley Fever Virus
736   Encephalitis. J Virol. 2018;92(24). Epub 20181127. doi: 10.1128/jvi.01270-18. PubMed PMID:
737   30258000; PubMed Central PMCID: PMCPMC6258944.
738   28.   Daffis S, Samuel MA, Suthar MS, Gale M, Jr., Diamond MS. Toll-like receptor 3 has a
739   protective role against West Nile virus infection. J Virol. 2008;82(21):10349-58. Epub
740   2008/08/22. doi: 10.1128/jvi.00935-08. PubMed PMID: 18715906; PubMed Central PMCID:
741   PMCPMC2573187.
742   29.   Town T, Bai F, Wang T, Kaplan AT, Qian F, Montgomery RR, et al. Toll-like receptor 7
743   mitigates lethal West Nile encephalitis via interleukin 23-dependent immune cell infiltration and
744   homing. Immunity. 2009;30(2):242-53. Epub 2009/02/10. doi: 10.1016/j.immuni.2008.11.012.
745   PubMed PMID: 19200759; PubMed Central PMCID: PMCPMC2707901.
746   30.   Suthar MS, Ma DY, Thomas S, Lund JM, Zhang N, Daffis S, et al. IPS-1 is essential for
747   the control of West Nile virus infection and immunity. PLoS Pathog. 2010;6(2):e1000757. Epub
748   2010/02/09. doi: 10.1371/journal.ppat.1000757. PubMed PMID: 20140199; PubMed Central
749   PMCID: PMCPMC2816698.
750   31.   Hise AG, Traylor Z, Hall NB, Sutherland LJ, Dahir S, Ermler ME, et al. Association of
751   Symptoms and Severity of Rift Valley Fever with Genetic Polymorphisms in Human Innate
752   Immune Pathways. PLoS Negl Trop Dis. 2015;9(3):e0003584. doi:
753   10.1371/journal.pntd.0003584.
754   32.   Roberts KK, Hill TE, Davis MN, Holbrook MR, Freiberg AN. Cytokine response in
755   mouse bone marrow derived macrophages after infection with pathogenic and non-pathogenic
756   Rift Valley fever virus. J Gen Virol. 2015;96(Pt 7):1651-63. Epub 2015/03/12. doi:
757   10.1099/vir.0.000119. PubMed PMID: 25759029; PubMed Central PMCID: PMCPMC4635452.
758   33.   Artegiani B, Lyubimova A, Muraro M, van Es JH, van Oudenaarden A, Clevers H. A
759   Single-Cell RNA Sequencing Study Reveals Cellular and Molecular Dynamics of the
760   Hippocampal Neurogenic Niche. Cell Rep. 2017;21(11):3271-84. doi:
761   10.1016/j.celrep.2017.11.050. PubMed PMID: 29241552.
762   34.   Cougnoux A, Yerger JC, Fellmeth M, Serra-Vinardell J, Martin K, Navid F, et al. Single
763   Cell Transcriptome Analysis of Niemann-Pick Disease, Type C1 Cerebella. Int J Mol Sci.
764   2020;21(15). Epub 20200728. doi: 10.3390/ijms21155368. PubMed PMID: 32731618; PubMed
765   Central PMCID: PMCPMC7432835.
766   35.   Vanlandewijck M, He L, Mäe MA, Andrae J, Ando K, Del Gaudio F, et al. A molecular
767   atlas of cell types and zonation in the brain vasculature. Nature. 2018;554(7693):475-80. Epub
768   20180214. doi: 10.1038/nature25739. PubMed PMID: 29443965.
769   36.   Hammond TR, Dufort C, Dissing-Olesen L, Giera S, Young A, Wysoker A, et al. Single-
770   Cell RNA Sequencing of Microglia throughout the Mouse Lifespan and in the Injured Brain
771   Reveals Complex Cell-State Changes. Immunity. 2019;50(1):253-71.e6. Epub 20181121. doi:
772   10.1016/j.immuni.2018.11.004. PubMed PMID: 30471926; PubMed Central PMCID:
773   PMCPMC6655561.
774   37.   Morimoto K, Nakajima K. Role of the Immune System in the Development of the Central
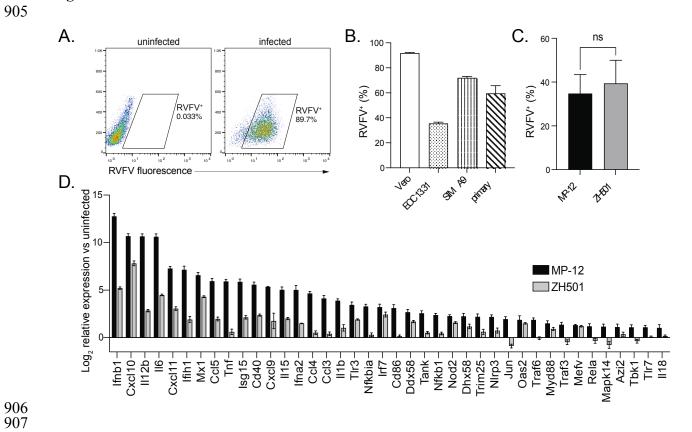775   Nervous System. Frontiers in Neuroscience. 2019;13(916). doi: 10.3389/fnins.2019.00916.

776 38.   Goldmann T, Wieghofer P, Jordão MJ, Prutek F, Hagemeyer N, Frenzel K, et al. Origin,
777 fate and dynamics of macrophages at central nervous system interfaces. Nat Immunol.
778 2016;17(7):797-805. Epub 2016/05/03. doi: 10.1038/ni.3423. PubMed PMID: 27135602;
779 PubMed Central PMCID: PMCPMC4968048.
780 39.   Masuda T, Tsuda M, Yoshinaga R, Tozaki-Saitoh H, Ozato K, Tamura T, et al. IRF8 is a
781 critical transcription factor for transforming microglia into a reactive phenotype. Cell Rep.
782 2012;1(4):334-40. Epub 2012/07/27. doi: 10.1016/j.celrep.2012.02.014. PubMed PMID:
783 22832225; PubMed Central PMCID: PMCPMC4158926.
784 40.   Masuda T, Iwamoto S, Mikuriya S, Tozaki-Saitoh H, Tamura T, Tsuda M, et al.
785 Transcription factor IRF1 is responsible for IRF8-mediated IL-1β expression in reactive
786 microglia. J Pharmacol Sci. 2015;128(4):216-20. Epub 2015/09/01. doi:
787 10.1016/j.jphs.2015.08.002. PubMed PMID: 26318672.
788 41.   Wierońska JM, Cieślik P, Kalinowski L. Nitric Oxide-Dependent Pathways as Critical
789 Factors in the Consequences and Recovery after Brain Ischemic Hypoxia. Biomolecules.
790 2021;11(8). Epub 20210726. doi: 10.3390/biom11081097. PubMed PMID: 34439764; PubMed
791 Central PMCID: PMCPMC8392725.
792 42.   Voskoboinik I, Whisstock JC, Trapani JA. Perforin and granzymes: function, dysfunction
793 and human pathology. Nature reviews Immunology. 2015;15(6):388-400. doi: 10.1038/nri3839.
794 PubMed PMID: 25998963.
795 43.   Shrestha B, Samuel MA, Diamond MS. CD8+ T cells require perforin to clear West Nile
796 virus from infected neurons. J Virol. 2006;80(1):119-29. doi: 10.1128/jvi.80.1.119-129.2006.
797 PubMed PMID: 16352536; PubMed Central PMCID: PMCPMC1317548.
798 44.   Shi F-D, Ransohoff RM. Nature killer cells in the central nervous system. Natural Killer
799 Cells. 2010:373-83. Epub 2010/01/29. doi: 10.1016/B978-0-12-370454-2.00028-4. PubMed
800 PMID: PMC7150147.
801 45.   Yao Y, Strauss-Albee DM, Zhou JQ, Malawista A, Garcia MN, Murray KO, et al. The
802 natural killer cell response to West Nile virus in young and old individuals with or without a
803 prior history of infection. PLOS ONE. 2017;12(2):e0172625. doi:
804 10.1371/journal.pone.0172625.
805 46.   Choi YH, Lim EJ, Kim SW, Moon YW, Park KS, An HJ. IL-27 enhances IL-15/IL-18-
806 mediated activation of human natural killer cells. J Immunother Cancer. 2019;7(1):168. Epub
807 20190705. doi: 10.1186/s40425-019-0652-7. PubMed PMID: 31277710; PubMed Central
808 PMCID: PMCPMC6612093.
809 47.   Ochayon DE, Waggoner SN. The Effect of Unconventional Cytokine Combinations on
810 NK-Cell Responses to Viral Infection. Frontiers in Immunology. 2021;12(775). doi:
811 10.3389/fimmu.2021.645850.
812 48.   Nakanishi K. Unique Action of Interleukin-18 on T Cells and Other Immune Cells.
813 Frontiers in Immunology. 2018;9(763). doi: 10.3389/fimmu.2018.00763.
814 49.   Ziblat A, Domaica CI, Spallanzani RG, Iraolagoitia XL, Rossi LE, Avila DE, et al. IL-27
815 stimulates human NK-cell effector functions and primes NK cells for IL-18 responsiveness.
816 European journal of immunology. 2015;45(1):192-202. Epub 20141202. doi:
817 10.1002/eji.201444699. PubMed PMID: 25308526.
818 50.   Smith DR, Steele KE, Shamblin J, Honko A, Johnson J, Reed C, et al. The pathogenesis
819 of Rift Valley fever virus in the mouse model. Virology. 2010;407(2):256-67. Epub 2010/09/21.
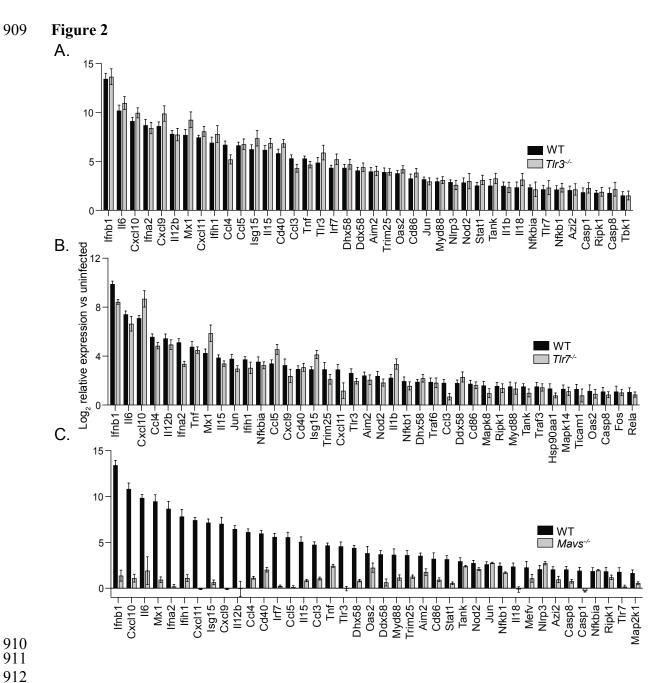820 doi: 10.1016/j.virol.2010.08.016. PubMed PMID: 20850165.

821   51.   Chen Z, Zhong D, Li G. The role of microglia in viral encephalitis: a review. Journal of
822   neuroinflammation. 2019;16(1):76. Epub 2019/04/11. doi: 10.1186/s12974-019-1443-2. PubMed
823   PMID: 30967139; PubMed Central PMCID: PMCPMC6454758.
824   52.   Stonedahl S, Clarke P, Tyler KL. The Role of Microglia during West Nile Virus Infection
825   of the Central Nervous System. Vaccines (Basel). 2020;8(3). Epub 2020/09/03. doi:
826   10.3390/vaccines8030485. PubMed PMID: 32872152; PubMed Central PMCID:
827   PMCPMC7563127.
828   53.   Pichlmair A, Lassnig C, Eberle CA, Górna MW, Baumann CL, Burkard TR, et al. IFIT1
829   is an antiviral protein that recognizes 5'-triphosphate RNA. Nat Immunol. 2011;12(7):624-30.
830   Epub 2011/06/07. doi: 10.1038/ni.2048. PubMed PMID: 21642987.
831   54.   Neil SJ, Zang T, Bieniasz PD. Tetherin inhibits retrovirus release and is antagonized by
832   HIV-1 Vpu. Nature. 2008;451(7177):425-30. Epub 2008/01/18. doi: 10.1038/nature06553.
833   PubMed PMID: 18200009.
834   55.   Radoshitzky SR, Dong L, Chi X, Clester JC, Retterer C, Spurgers K, et al. Infectious
835   Lassa virus, but not filoviruses, is restricted by BST-2/tetherin. J Virol. 2010;84(20):10569-80.
836   Epub 2010/08/06. doi: 10.1128/jvi.00103-10. PubMed PMID: 20686043; PubMed Central
837   PMCID: PMCPMC2950602.
838   56.   Lucas TM, Richner JM, Diamond MS, Perlman S. The Interferon-Stimulated Gene
839   <i>Ifi27l2a</i> Restricts West Nile Virus Infection and Pathogenesis in a Cell-Type- and
840   Region-Specific Manner. Journal of Virology. 2016;90(5):2600-15. doi: doi:10.1128/JVI.02463-
841   15.
842   57.   Lee MS, Kim B, Oh GT, Kim Y-J. OASL1 inhibits translation of the type I interferon–
843   regulating transcription factor IRF7. Nature Immunology. 2013;14(4):346-55. doi:
844   10.1038/ni.2535.
845   58.   Zhao J, Vijay R, Zhao J, Gale M, Jr., Diamond MS, Perlman S. MAVS Expressed by
846   Hematopoietic Cells Is Critical for Control of West Nile Virus Infection and Pathogenesis. J
847   Virol. 2016;90(16):7098-108. Epub 20160727. doi: 10.1128/jvi.00707-16. PubMed PMID:
848   27226371; PubMed Central PMCID: PMCPMC4984631.
849   59.   O'Keefe GM, Nguyen VT, Ping Tang L, Benveniste EN. IFN-γ Regulation of Class II
850   Transactivator Promoter IV in Macrophages and Microglia: Involvement of the Suppressors of
851   Cytokine Signaling-1 Protein. The Journal of Immunology. 2001;166(4):2260-9. doi:
852   10.4049/jimmunol.166.4.2260.
853   60.   Harmon B, Schudel BR, Maar D, Kozina C, Ikegami T, Tseng CT, et al. Rift Valley fever
854   virus strain MP-12 enters mammalian host cells via caveola-mediated endocytosis. J Virol.
855   2012;86(23):12954-70. Epub 20120919. doi: 10.1128/jvi.02242-12. PubMed PMID: 22993156;
856   PubMed Central PMCID: PMCPMC3497621.
857   61.   Harmon B, Bird SW, Schudel BR, Hatch AV, Rasley A, Negrete OA. A Genome-Wide
858   RNA Interference Screen Identifies a Role for Wnt/β-Catenin Signaling during Rift Valley Fever
859   Virus Infection. J Virol. 2016;90(16):7084-97. Epub 20160727. doi: 10.1128/jvi.00543-16.
860   PubMed PMID: 27226375; PubMed Central PMCID: PMCPMC4984662.
861   62.   Rasley A, Anguita J, Marriott I. Borrelia burgdorferi induces inflammatory mediator
862   production by murine microglia. Journal of neuroimmunology. 2002;130(1):22-31. doi:
863   https://doi.org/10.1016/S0165-5728(02)00187-X.
864   63.   Rasley A, Bost KL, Olson JK, Miller SD, Marriott I. Expression of functional NK-1
865   receptors in murine microglia. Glia. 2002;37(3):258-67. doi: https://doi.org/10.1002/glia.10034.

866   64.   Martin E, El-Behi M, Fontaine B, Delarasse C. Analysis of Microglia and Monocyte-
867   derived Macrophages from the Central Nervous System by Flow Cytometry. Journal of
868   visualized experiments : JoVE. 2017;(124):55781. doi: 10.3791/55781. PubMed PMID:
869   28671658.
870   65.   Bird BH, Bawiec DA, Ksiazek TG, Shoemaker TR, Nichol ST. Highly sensitive and
871   broadly reactive quantitative reverse transcription-PCR assay for high-throughput detection of
872   Rift Valley fever virus. J Clin Microbiol. 2007;45(11):3506-13. Epub 2007/09/07. doi:
873   10.1128/jcm.00936-07. PubMed PMID: 17804663; PubMed Central PMCID:
874   PMCPMC2168471.
875   66.   Dobin A, Davis CA, Schlesinger F, Drenkow J, Zaleski C, Jha S, et al. STAR: ultrafast
876   universal RNA-seq aligner. Bioinformatics. 2013;29(1):15-21. Epub 20121025. doi:
877   10.1093/bioinformatics/bts635. PubMed PMID: 23104886; PubMed Central PMCID:
878   PMCPMC3530905.
879   67.   Liao Y, Smyth GK, Shi W. featureCounts: an efficient general purpose program for
880   assigning sequence reads to genomic features. Bioinformatics. 2014;30(7):923-30. Epub
881   20131113. doi: 10.1093/bioinformatics/btt656. PubMed PMID: 24227677.
882   68.   Risso D, Ngai J, Speed TP, Dudoit S. Normalization of RNA-seq data using factor
883   analysis of control genes or samples. Nature biotechnology. 2014;32(9):896-902. Epub
884   2014/08/24. doi: 10.1038/nbt.2931. PubMed PMID: 25150836.
885   69.   Robinson MD, McCarthy DJ, Smyth GK. edgeR: a Bioconductor package for differential
886   expression analysis of digital gene expression data. Bioinformatics (Oxford, England).
887   2010;26(1):139-40. Epub 2009/11/11. doi: 10.1093/bioinformatics/btp616. PubMed PMID:
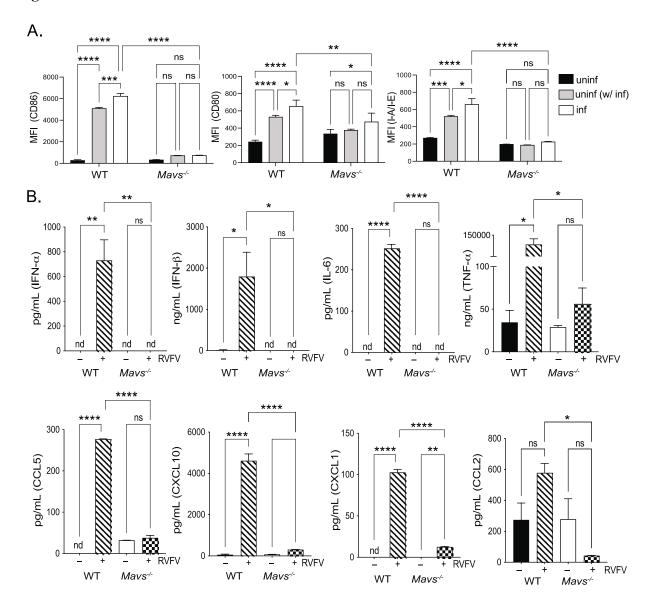888   19910308.
889   70.   Chen J, Bardes EE, Aronow BJ, Jegga AG. ToppGene Suite for gene list enrichment
890   analysis and candidate gene prioritization. Nucleic Acids Res. 2009;37(Web Server
891   issue):W305-W11. Epub 2009/05/22. doi: 10.1093/nar/gkp427. PubMed PMID: 19465376.
892   71.   Brewer GJ, Torricelli JR. Isolation and culture of adult neurons and neurospheres. Nature
893   Protocols. 2007;2(6):1490-8. doi: 10.1038/nprot.2007.207.
894   72.   Stuart T, Butler A, Hoffman P, Hafemeister C, Papalexi E, Mauck WM, 3rd, et al.
895   Comprehensive Integration of Single-Cell Data. Cell. 2019;177(7):1888-902.e21. Epub
896   2019/06/11. doi: 10.1016/j.cell.2019.05.031. PubMed PMID: 31178118; PubMed Central
897   PMCID: PMCPMC6687398.
898   73.   Hum NR, Sebastian A, Gilmore SF, He W, Martin KA, Hinckley A, et al. Comparative
899   Molecular Analysis of Cancer Behavior Cultured In Vitro, In Vivo, and Ex Vivo. Cancers
900   (Basel). 2020;12(3). Epub 20200314. doi: 10.3390/cancers12030690. PubMed PMID: 32183351;
901   PubMed Central PMCID: PMCPMC7140030.
902
903
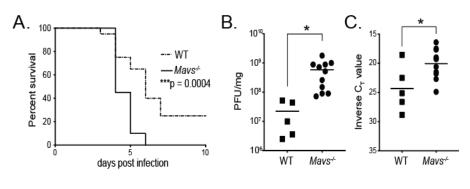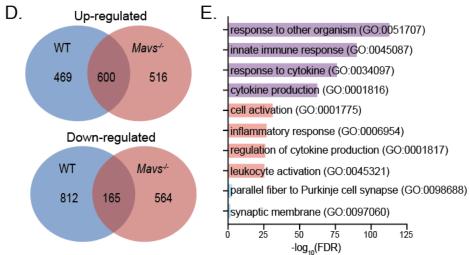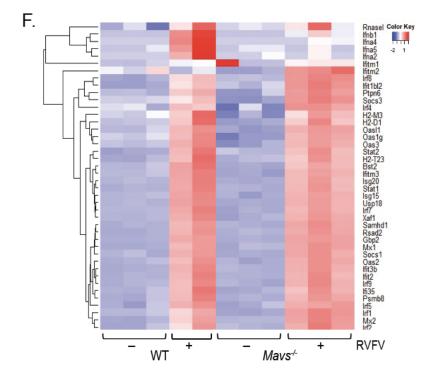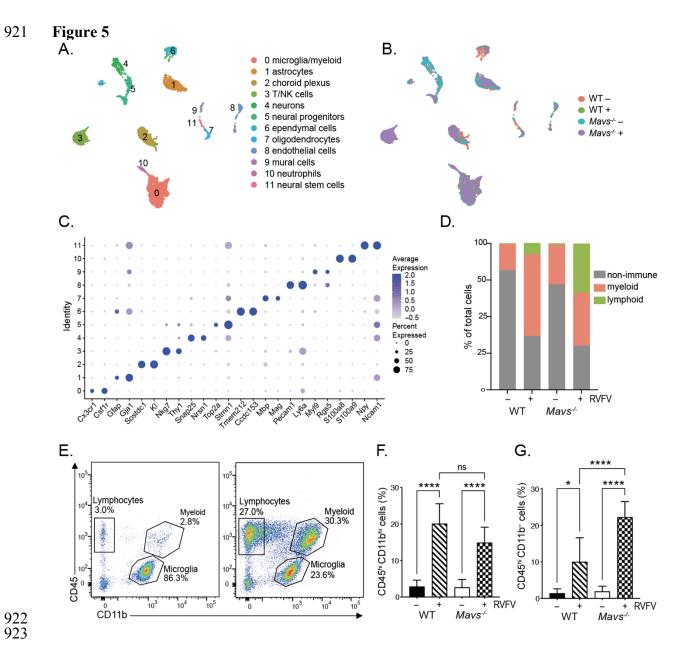
904 **Figure 1**
905

906
907
908

909 **Figure 2**

Figure 3

917 **Figure 4**
918

919
920

921 **Figure 5**

922
923

924 **Figure 6**

925

926
927

928 **Figure 7**

929

930
931
932
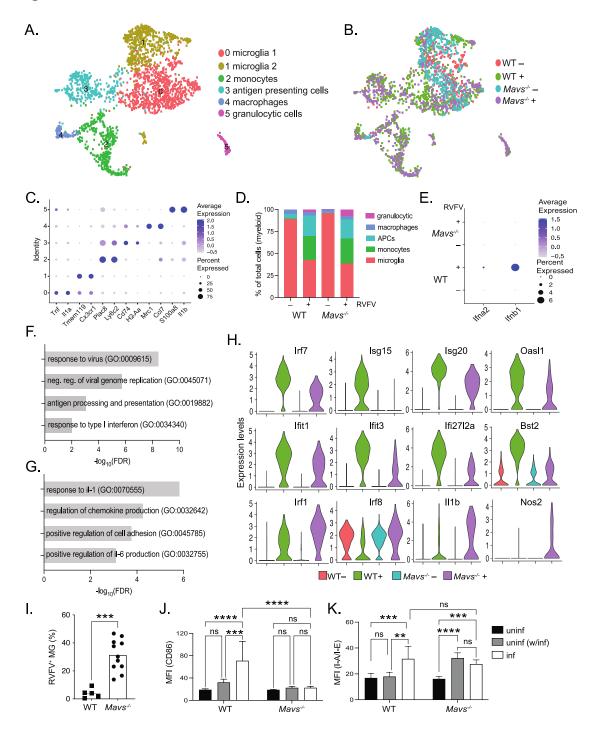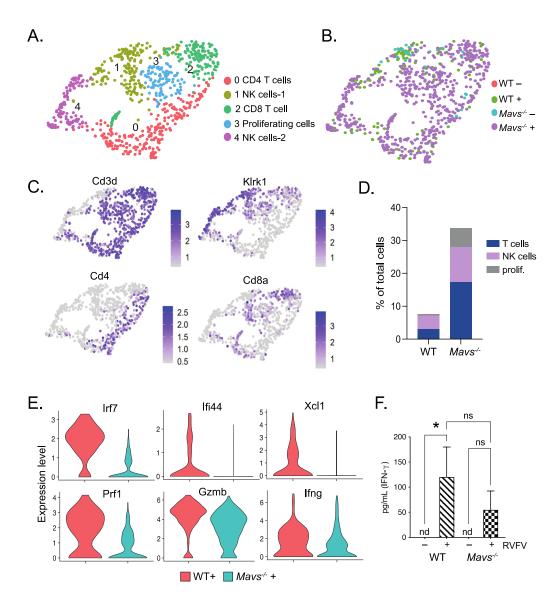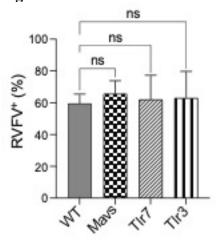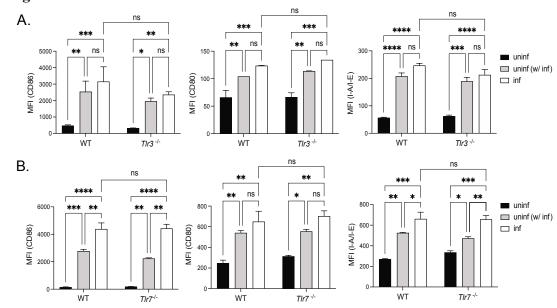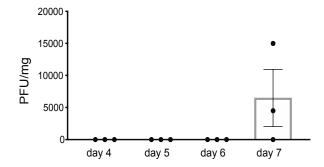
Figure S1

Figure S2

Figure S3

943
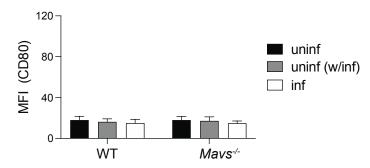944 **Figure S4**

945
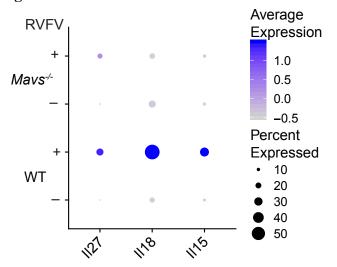946
947 **Figure S5**

948
949
950

951 **Figure 1. RVFV infects microglia.** Microglia cell lines EOC 13.31 and SIM A9 and primary
952 microglia derived from the brains of neonatal mice, along with Vero positive control cells, were
953 infected with RVFV MP-12. The percentage of cells positive for RVFV was assessed by flow
954 cytometry. Representative plots of Vero cell infection analysis (A). RVFV infection rate for all
955 cell types (B). Primary microglia derived from wildtype (WT) mice were infected with RVFV
956 MP-12 or ZH501 and the percentage of cells positive for RVFV was assessed by flow cytometry
957 (C). The relative expression of 40 antiviral response genes with the highest fold change in
958 infected versus uninfected cells (D). Data in (B-C) are shown as the mean +/- SD. Data in (D) are
959 shown as the mean $\log_2$ fold change in infected versus uninfected cells +/- SEM.
960
961 **Figure 2. Microglial response to RVFV infection is dependent upon MAVS and**
962 **independent of TLR7 and TLR3.** Primary microglia derived from WT or *Tlr3*^{-/-} (A), *Tlr7*^{-/-} (B)
963 or *Mavs*^{-/-} (C) were infected with RVFV MP-12. The relative expression of 40 antiviral response
964 genes with the highest fold change in WT cells are shown as the mean $\log_2$ fold change in
965 infected versus uninfected cells, +/- SEM.
966
967 **Figure 3. Microglia respond to RVFV infection in vitro by cytokine secretion and**
968 **upregulation of activation markers.** Microglia derived from WT or *Mavs*^{-/-} mice were infected
969 with RVFV MP-12 and at 18-24 h post-infection, cells and cellular supernatants were harvested
970 for flow cytometry and multiplex cytokine analysis, respectively. The expression levels of the
971 indicated activation markers were assessed on uninfected cells (black bars), uninfected cells in
972 culture with infected cells (uninf (w/ inf), gray bars), and infected cells (inf, white bars) and
973 shown as the mean fluorescence intensity of the indicated activation markers (A). Cytokine
974 levels in cellular supernatants (B). Data are shown as the mean +/- SD, nd = not detected and
975 was denoted as zero *p <0.05, **p<0.01, ***p<0.001, ****p<0.0001
976
977 **Figure 4. *Mavs*^{-/-} mice are more susceptible to intranasal RVFV infection and display**
978 **increased viral burden and immune gene expression in the brain.** WT or *Mavs*^{-/-} mice were
979 infected intranasally with 1000 PFU RVFV ZH501 (A), or 5x10^{5} PFU RVFV MP-12 (B-E).
980 Morbidity and mortality were assessed daily, and percent survival is depicted in (A). On day 7
981 post infection (B-E), brains were processed for viral quantitation and RNA extraction. Viral
982 quantitation (B). Genes differentially expressed between uninfected and infected brains (C).
983 Functional enrichment of differentially expressed genes (D). Ontologies that were enriched in
984 both WT and *Mavs*^{-/-} infected brains are highlighted in purple. Pathways enriched only in *Mavs*^{-/-}
985 or WT infected brains are highlighted in red and blue, respectively. Heatmap of IFN α/β
986 signaling genes (E). *p<0.05, ***p<0.001
987
988 **Figure 5. Single cell RNA sequencing reveals shifts in cell populations and immune**
989 **infiltration in the brain following RVFV infection.** UMAP plots depicting cell clusters derived
990 from WT and *Mavs*^{-/-} brains, +/- RVFV infection. Cell types (A) or conditions (B) are color
991 coded. Gene markers for specific cell types (C). The distribution of cell types within brains of
992 each condition (D). Flow cytometry: Representative plots of CD11b vs CD45 and the gates
993 defining microglia, lymphocytes, and myeloid cells are shown for uninfected (left panel) and
994 infected brains (right panel) (E). The percent myeloid cells (CD11b^{hi} CD45^{hi}), and lymphocytes
995 (CD11b^{-} CD45^{hi}) (F) and (G), respectively. Data in (F) and (G) are shown as the mean +/- SD.
996 *p<0.05, ***p<0.001, ****p<0.0001

997

998 **Figure 6. Microglia from *Mavs*$^{-/-}$ brains have defective response to RVFV infection**
999 UMAP plots depicting cell clusters of myeloid lineage cells derived from WT and *Mavs*$^{-/-}$ brains,
1000 +/- RVFV infection. Cell types (A) or conditions (B) are color coded. Gene markers for specific
1001 cell types (C). The distribution of myeloid lineage cell types within brains of each condition (D).
1002 Expression of type I IFNs within microglia (clusters 0 and 1) (E). Gene ontology (GO)
1003 enrichment analysis showing enriched in WT vs *Mavs*$^{-/-}$, or *Mavs*$^{-/-}$ vs WT microglia (clusters 0
1004 and 1) from infected brains are shown in (F) and (G), respectively. Violin plots depicting the
1005 relative expression of selected genes within microglia (clusters 0 and 1) are shown in (H). Flow
1006 cytometry: microglia were defined as CD11b^{int} CD45^{int} as described in Figure 5, and the
1007 percentage of RVFV$^+$ microglia are shown in (I). Mean fluorescence intensities (MFI) of CD86
1008 and I-A/I-E expression on microglia (J) and (K), respectively. Data in (I-K) are shown as the
1009 mean +/- SD. **p<0.01, ***p<0.001, ****p<0.0001

1010

1011 **Figure 7. Dysregulated pattern of lymphocyte infiltration and gene expression in brains of**
1012 ***Mavs*$^{-/-}$ mice.** UMAP plots depicting cell clusters of lymphoid lineage cells derived from WT and
1013 *Mavs*$^{-/-}$ brains, +/- RVFV infection. Cell types (A) or conditions (B) are color coded. Feature
1014 plots showing expression of cell type specific markers are shown in (C). The distribution of
1015 lymphoid lineage cell types within brains of infected mice (D). Violin plots depicting the relative
1016 expression of selected genes within all lymphocytes are shown in (E). Quantitation of IFN-γ is
1017 depicted in (F). *p<0.05

1018

1019 **Figure S1. Infection of primary microglia is not dependent upon genotype.** Primary
1020 microglia derived from WT or the indicated genetically deficient mice were infected with RVFV
1021 MP-12 and the percentage of cells positive for RVFV was assessed by flow cytometry.

1022

1023 **Figure S2. Expression of activation markers is not dependent on TLR3 or TLR7.** Microglia
1024 derived from WT or *Tlr3*$^{-/-}$ (A) or *Tlr7*$^{-/-}$ (B) mice were infected with RVFV MP-12 and at 18-24
1025 hours post-infection, cells were harvested for flow cytometry. The expression levels of the
1026 indicated activation markers were assessed on uninfected cells (black bars), uninfected cells in
1027 culture with infected cells (uninf (w/ inf), gray bars), and infected cells (inf, white bars) and
1028 shown as the mean fluorescence intensity of the indicated activation markers. Data are shown as
1029 the mean +/- SD *p <0.05, **p<0.01, ***p<0.001, ****p<0.0001

1030

1031 **Figure S3. RVFV is detected in the brain on day 7 post infection.** WT mice were infected
1032 intranasally with 5x10^5 PFU RVFV MP-12 and brains were harvested on the indicated day post
1033 infection for viral quantitation.

1034

1035 **Figure S4. CD80 expression on microglia.** Mean fluorescence intensity of CD80 on microglia
1036 isolated from the brains of WT and *Mavs*$^{-/-}$ mice, +/- RVFV infection.

1037

1038 **Figure S5. Microglia and myeloid cells from *Mavs*$^{-/-}$ infected brains display lower levels of**
1039 **cytokine gene expression.**
1040